Hypertrophy induced KIF5B controls mitochondrial localization and function in neonatal rat cardiomyocytes

Tigchelaar, Wardit; de Jong, Anne Margreet; Bloks, Vincent W.; Gilst, van, Wiek H.; de Boer, Rudolf A.; Sillje, Herman H. W.

Published in:
Journal of molecular and cellular cardiology

DOI:
10.1016/j.yjmcc.2016.04.005

Publication date:
2016

Journal of Molecular and Cellular Cardiology 97 (2016) 70–81

Contents lists available at ScienceDirect

Journal of Molecular and Cellular Cardiology

journal homepage: www.elsevier.com/locate/yjmcc

Hypertrophy induced KIF5B controls mitochondrial localization and function in neonatal rat cardiomyocytes

Wardit Tigchelaar [a,1], Anne Margreet de Jong [a,1], Vincent W. Bloks [b], Wiek H. van Gilst [a], Rudolf A. de Boer [a], Herman H.W. Silljé [a,*]

[a] Department of Cardiology, University Medical Center Groningen, University of Groningen, The Netherlands
[b] Paediatrics, University Medical Center Groningen, University of Groningen, The Netherlands

ARTICLE INFO

Article history:
Received 9 December 2015
Received in revised form 27 March 2016
Accepted 12 April 2016
Available online 17 April 2016

Keywords:
Cardiomyocyte
Hypertrophy
Mitochondria
Kif5b
Heart

ABSTRACT

Cardiac hypertrophy is associated with growth and functional changes of cardiomyocytes, including mitochondrial alterations, but the latter are still poorly understood. Here we investigated mitochondrial function and dynamic localization in neonatal rat ventricular cardiomyocytes (NRVCs) stimulated with insulin like growth factor 1 (IGF1) or phenylephrine (PE), mimicking physiological and pathological hypertrophic responses, respectively. A decreased activity of the mitochondrial electron transport chain (ETC) (state 3) was observed in permeabilized NRVCs stimulated with PE, whereas this was improved in IGF1 stimulated NRVCs. In contrast, in intact NRVCs, mitochondrial oxygen consumption rate (OCR) was increased in PE stimulated NRVCs, but remained constant in IGF1 stimulated NRVCs. After stimulation with PE, mitochondria were localized to the periphery of the cell. To study the differences in more detail, we performed gene array studies. IGF1 and PE stimulated NRVCs did not reveal major differences in gene expression of mitochondrial encoding proteins, but we identified a gene encoding a motor protein implicated in mitochondrial localization, kinesin family member 5b (*Kif5b*), which was clearly elevated in PE stimulated NRVCs but not in IGF1 stimulated NRVCs. We confirmed that *Kif5b* gene and protein expression were elevated in animal models with pathological cardiac hypertrophy. Silencing of *Kif5b* reverted the peripheral mitochondrial localization in PE stimulated NRVCs and diminished PE induced increases in mitochondrial OCR, indicating that KIF5B dependent localization affects cellular responses to PE stimulated NRVCs.

These results indicate that KIF5B contributes to mitochondrial localization and function in cardiomyocytes and may play a role in pathological hypertrophic responses in vivo.

1. Introduction

Cardiac hypertrophy is believed to be an adaptive response of the heart aimed at reducing wall stress and maintaining cardiac function. Cardiac hypertrophy can be broadly divided into pathological and physiological hypertrophy. Both types of hypertrophy are associated with growth and functional changes of cardiomyocytes, but pathological hypertrophy may result in cardiac decompensation and heart failure [1,2].

Physiological hypertrophy can be induced by growth factors, like insulin-like growth factor (IGF1), whereas adrenergic signaling and angiotensin II can stimulate pathological hypertrophy. Although the common outcome of these hypertrophic signals is cardiomyocyte growth (hypertrophy), these responses are associated with distinct intracellular signaling pathways and different structural and functional consequences [3]. Among different events, like fibrosis and microvascular abnormalities [3,4], energy metabolic reprogramming also appears to be disparate between the two hypertrophic conditions [5]. This includes alterations in substrate usage and mitochondrial function [3]. The metabolic switch from fatty acids to glucose usage, which is observed in pathological hypertrophy, has been investigated in great detail [6–8]. The changes in mitochondrial dynamics and function on the other hand are still vague. The general view is that physiological factors stimulate mitochondrial biogenesis and hence mitochondrial capacity [9], whereas pathological stimulation results in altered mitochondrial dynamics and activity [10]. These changes are still far from understood and differences in etiology, hypertrophic state (compensated/decompensated) and methodology have probably contributed to different results [11]. Moreover, the complexity of the cardiovascular system in which (neuro)hormonal signals, biomechanical changes,

* Corresponding author at: Department of Cardiology, University Medical Center Groningen, University of Groningen, Hanzeplein 1, 9713 GZ Groningen, P.O. Box 30.001, 9700 RB Groningen, The Netherlands.
E-mail address: h.h.w.sillje@umcg.nl (H.H.W. Silljé).
[1] These authors contributed equally to this work.

http://dx.doi.org/10.1016/j.yjmcc.2016.04.005

hemodynamic effects and altered substrate availability all have an impact on hypertrophy development and mitochondrial function most likely hampers these studies.

In this study we aimed to investigate mitochondrial function in a simplified system using cultured neonatal rat cardiomyocytes (NRVCs) and mimicked physiological and pathological hypertrophy with IGF1 and phenylephrine (PE), respectively. We show that a pathological stimulus (PE) can induce changes in mitochondrial function and dynamic localization within 24 h of stimulation. In contrast to IGF1 stimulated NRVCs, in PE stimulated NRVCs the kinesin motor protein KIF5B was upregulated. This results in abnormal and more peripheral localization of the mitochondria. Depletion of KIF5B prevented this mitochondrial redistribution and also partially inhibits the mitochondrial respiratory increase and hypertrophic response observed after stimulation with PE. This indicates that KIF5B is involved in PE induced changes in mitochondrial localization and function and suggests that KIF5B could play a role in energetic changes in pathological hypertrophic responses.

2. Materials and methods

2.1. Ethics statement

All experiments were approved by the Committee on Animal Experimentation of the University of Groningen and were conducted under international guidelines on animal experimentation conforming to the Guide for the Care and Use of Laboratory Animals published by the Directive 2010/63/EU of the European Parliament.

2.2. Isolation and culturing of primary cardiomyocytes

Primary neonatal rat ventricular cardiomyocytes (NRVCs) were isolated from Sprague Dawley neonatal rats of 1–3 days old, as previously described [12,13]. NRVCs were grown in Dulbecco's Modified Eagle Medium (DMEM) supplemented with 5% fetal calf serum (FCS) and penicillin–streptomycin (100 U/ml–100 μg/ml). NRVCs were serum starved in DMEM with penicillin–streptomycin (100 U/ml–100 μg/ml) 48 h after isolation. After 24 h of starvation NRVCs were stimulated with 50 μM phenylephrine (PE) or 10 nM insulin-like growth factor 1 (IGF1) (Life Technologies) for 24 h. All media and supplements were purchased from Sigma-Aldrich Chemie B.V., Zwijndrecht, The Netherlands. After stimulation, NRVCs were washed twice with PBS and used for further analysis.

2.3. Immunofluorescence microscopy

NRVCs were grown on coverslips coated with laminin (Millipore, Amsterdam, The Netherlands) and treated as described above. NRVCs were fixed for 10 min with 4% paraformaldehyde at 4 °C, followed by permeabilization with 0.3% Triton X for 5 min. For cell size measurements, NRVCs were incubated with monoclonal anti-alpha-actinin antibody (Sigma-Aldrich Chemie B.V., Zwijndrecht, The Netherlands) in 3% BSA, 2% normal goat serum, and 0.1% Tween in PBS for 1 h at RT. NRVCs were washed with PBS and incubated for another hour with a goat anti-mouse fluorescein isothiocyanate (FITC) secondary antibody (Santa-Cruz Biotechnology, Heidelberg, Germany). Coverslips were mounted with mounting medium containing 4′,6-diamidino-2-phenylindole dihydrochloride (DAPI) (Vector Laboratories, Burlingame, CA, USA) for counterstaining of the nuclei. Slides were imaged using a Leica DMI6000B inverted immunofluorescence microscope and cell size was determined using ImageJ analysis software. To determine mitochondrial localization the same staining protocol was followed as described above, but next to alpha-actinin staining, anti-TOM20 antibody staining was performed (Santa Cruz, Heidelberg, Germany). To obtain a quantitative measure of mitochondrial distribution in the cytosol, the intensity of TOM20 staining was determined in a circular area at the nuclear periphery (perinuclear) and an identical sized area at the cell membrane (cellular periphery) using ImageJ software. These regions were never overlapping. The intensity ratio for perinuclear versus peripheral TOM20 staining was determined and at least 25 NRVCs/condition were analyzed in at least three independent experiments. The percentage of NRVCs with a perinuclear to peripheral ratio above 3.0 was determined. Detailed microscopy images were generated using a Delta Vision Elite system using a 60× objective at the UMCG imaging center. Z-stacks were generated and images were deconvolved by 5 iterations and subsequently a Z-projection was generated.

2.4. [3H]-leucine incorporation

NRVCs were grown in 12-well plates and L-[4.5-^{3}H]leucine (1 μCi/ml, PerkinElmer) was added to the medium right after stimulation with PE or IGF1. NRVCs were cultured for an additional 24 h and L-[4.5-^{3}H]leucine incorporation was determined as previously described [12].

2.5. Quantitative real time PCR

Total RNA was isolated using a nucleospin RNA II kit (Bioke, Leiden, The Netherlands) and cDNA was synthesized using QuantiTect Reverse Transcriptional kit (Qiagen, Venlo, The Netherlands) according to the manufacturer's instructions. Relative gene expression was determined by quantitative real time PCR (qRT-PCR) on the Bio-Rad CFX384 real time system (Bio-Rad, Veenendaal, The Netherlands) using ABsolute QPCR SYBR Green mix (Thermo Scientific, Landsmeer, The Netherlands). Gene expressions were corrected for reference gene values (*Rplp0*), and expressed relative to the control group. Primer sequences used are depicted in Supplemental Table 1.

2.6. Western blot

Western blotting was performed as described previously [14]. In brief, protein was isolated with radio-immunoprecipitation assay (RIPA) buffer (50 mM Tris pH 8.0, 1% nonidet P40, 0.5% deoxycholate, 0.1% SDS, 150 mM NaCl) supplemented with 40 μl/ml phosphatase inhibitor cocktail 1 (Sigma-Aldrich Chemie B.V., Zwijndrecht, The Netherlands), 10 μl/ml protease inhibitor cocktail (Roche Diagnostics Corp., Indianapolis, IN, USA) and 1 mM phenylmethylsulfonyl fluoride (PMSF) (Roche Diagnostics Corp., Indianapolis, IN, USA). Protein concentrations were determined with a DC protein assay kit (Bio-Rad, Veenendaal, The Netherlands). Equal amounts of proteins were separated by SDS-PAGE and proteins were transferred onto polyvinylidene difluoride (PVDF) membranes. (The following antibodies were used: anti-OXPHOS cocktail (MitoSciences, Eugene, Oregon, USA), anti-pAKT (Cell Signaling Technology Danvers, MA, USA), anti-total AKT (Cell Signaling Technology Danvers, MA, USA), anti-beta-actin (Sigma-Aldrich Chemie B.V., Zwijndrecht, The Netherlands), anti-Kif5b anti-Mitofusin-1 (Abcam Cambridge, UK), anti-Drp1 (Becton Dickinson, Breda, The Netherlands) and anti-TOM20 (Santa Cruz, Heidelberg, Germany). After incubation with HRP-conjugated secondary antibodies, signals were visualized with ECL and analyzed with densitometry (ImageQuant LAS4000, GE Healthcare Europe, Diegem, Belgium). Cardiac troponin T (cTnT) was used as a loading control as described before [15].

2.7. Seahorse mitochondrial flux analyses

To determine the mitochondrial oxygen consumption rate (OCR) a Seahorse metabolic flux analyzer (Seahorse Biosciences, Massachusetts, USA) was used. A standardized protocol [16] was used to determine specific mitochondrial complex activities in permeabilized cells. To measure complex I and complex II mediated respiratory activities, cardiomyocytes were permeabilized using recombinant perfringolysin O (rPFO) (XF-plasma membrane permeabilizer (PMP) reagent)

(Seahorse Biosciences, Massachusetts, USA). NRVCs were cultured as described above. On the day of analysis, NRVCs were washed twice with ASBSA (70 mM sucrose, 220 mM mannitol, 10 mM KH_2PO_4, 5 mM KOH, 0.4% BSA). The XFPMP reagent (1 nM) was added together with the appropriate substrates and inhibitors and the assay was started immediately. To measure complex I activity, pyruvate (5 mM) and malate (2.5 mM) were added to the MAS–BSA solution. For complex II mediated respiration rotenone (1 μM) and succinate (10 mM) were used. The OCR was measured by adding subsequently ADP (1 mM), oligomycin (1 μg/μl) and FCCP (1 μM). Non-mitochondrial OCR was measured after the addition of antimycin/rotenone (1 μM/1 μM). This non-mitochondrial respiration was subtracted from the total OCR values resulting in ADP induced state 3 mitochondrial OCR, ATP-linked state 4 mOCR and FCCP induced uncoupled mOCR (state 3u).

Determination of the OCR in intact cardiomyocytes with the Seahorse metabolic flux analyzer was performed as previously described [17]. Neonatal cardiomyocytes were seeded at a density of 100,000 NRVCs/well in special Seahorse 24-well plates. One hour before initiation of measurements, medium was replaced with XF medium supplemented with 10 mM glucose or 1 mM pyruvate and incubated for 1 h in a CO_2 free 37 °C incubator. The basal respiration of the NRVCs was measured, followed by injection of oligomycin (ATP synthase inhibitor) (1 μM) to measure the ATP linked OCR. The uncoupler carbonyl cyanide 4-(trifluoromethoxy)phenylhydrazone (FCCP) (0.5 μM) was used to determine maximal respiration. Finally, rotenone (1 μM) and antimycin A (AR) (1 μM) were injected to determine the non-mitochondrial respiration via inhibition of complexes I and III, respectively. Mitochondrial specific OCR (mOCR) was calculated by subtracting the non-mitochondrial respiration AR of the total OCR values. ATP-linked OCR is the calculated difference between basal mOCR and mOCR after the addition of oligomycin. In each plate the same treatment was performed in triplicate or quadruple. The OCR was corrected for the amount of total protein per well as determined using the Biorad DC Protein Assay (Biorad).

2.8. mtDNA/nDNA ratio

Total DNA, including mitochondrial DNA (mtDNA), was extracted from NRVCs using the DNA blood and tissue kit (Qiagen, Venlo, The Netherlands). The isolated DNA showed high purity (A260/A280 > 1.8), as determined by spectroscopic analysis. To determine the ratio between mitochondrial and nuclear DNA, relative gene expression was determined by qRTPCR on a Bio-Rad CFX384 real time system using SYBR Green dye. The expression of the mitochondrial gene cytochrome b (*CytB*) was corrected for the expression of the nuclear gene *Trpm2*. Primers and procedure have been described before [17].

2.9. Citrate synthase activity

Whole cell citrate synthase activity was measured using an enzyme assay kit (Sigma-Aldrich Chemie B.V., Zwijndrecht, The Netherlands) according to the manufacturer's instructions and as previously described by us [17]. In short, cell lysates were prepared using the CelLytic M Cell Lysis Reagent and protein concentrations were measured. 3 μg of protein was combined with acetyl coenzyme A, 5,5′-dithiobis-(2-nitrobenzoic acid) (DTNB) and assay buffer in a 96 well plate. The reaction was initiated by adding oxaloacetate into the mixture and total activity was measured. Absorbance was measured at 412 nm using a spectrophotometer following a kinetic program. Triplicate measurements were performed on each sample.

2.10. Gene array

RNA was isolated as described above and 4 independent biological samples per condition were used for whole genome expression analysis. Biotin-labeling, hybridization, washing and scanning of GeneChip Rat Gene 1.1 ST arrays (Affymetrics) were performed in expert labs (Nutrigenomics Consortium, Wageningen, The Netherlands) according to Affymetrix's protocols. Processing of the data occurred using the MADMAX pipeline [18]. Array data have been deposited at the Gene Expression Omnibus (GEO) database (GSE73896). Differentially expressed gene sets were identified with the IBMT regularized t-test [19]. Corrections for multiple testing were done using the false discovery rate method [20]. A false discovery rate (FDR) of <10% was considered significantly changed. Genes related to the mitochondria were selected from the gene list with significantly regulated genes (FDR < 10%). These genes were annotated in biological processes using Database for Annotation, Visualization and Integrated Discovery (DAVID) software [21]. Biological processes shown are based on Gene Ontology, GOTERM_BP4. Gene set enrichment analysis [22] was performed to be able to detect significant pathway regulation of gene sets, thereby not only focusing on significantly regulated genes, but taking into account all expressed genes. A heat map was generated using statistical and graphical computer software "R". For the heat map only motor protein encoding genes were selected that we identified in the FDR < 10% gene lists.

2.11. Animal experiments

Expression of *Kif5b* was analyzed in multiple hypertrophy animal models. In all animal experiments, animals were kept on a 12 h light:12 h dark cycle with ad libitum access to food and water. Pressure overload in male C57BL/6J mice (Harlan, The Netherlands) was induced at the age of 8–10 weeks by transverse aortic constriction (TAC). Mice were terminated at 4 or 8 weeks post-TAC and sham operated animals were used as controls, as described previously [23]. Homozygous transgenic TGR (mREN2)27 rats overexpress mouse renin resulting in hypertension and consequently develop cardiac hypertrophy were used as described before [13,14,24]. Age- and gender-matched Sprague Dawley (SD) animals (genetic background strain) served as controls. For induction of physiological hypertrophy, male C57BL/6J mice were allowed voluntary wheel running for 10 weeks. Sedentary animals were used as controls.

2.12. Gene silencing

Silencing of gene expression was performed with oligofectamine (Dharmacon) according to the manufacturer's instruction. Silencing was performed with AccuTarget predesigned siRNA 1,664,194 and 1,664,195 from Bioneer targeting rat *Kif5b*. Control Accutarget siRNA sequences were also from Bioneer and have been described before [17].

2.13. Statistical analysis

All values are presented as means ± standard deviation (SD). Comparison of two groups was done using a two-tailed Student's t-test. One-way ANOVA with posthoc Bonferroni correction was used to compare the difference between multiple groups. When data were not normally distributed, a Kruskal Wallis test was performed, followed by a Mann–Whitney U test for individual comparison of means. SPSS software (PASW Statistics 22) was used for the statistical analyses. $P < 0.05$ was considered to be significant.

3. Results

3.1. PE and IGF1 induce different pathways, resulting in similar hypertrophic responses in NRVCs

Stimulation of NRVCs with IGF1 and PE resulted in a similar increase in cell size as is shown in Fig. 1A and B. Also protein synthesis was significantly increased upon stimulation with PE and IGF1, albeit somewhat stronger with IGF1 (Fig. 1C). The pathological stress markers

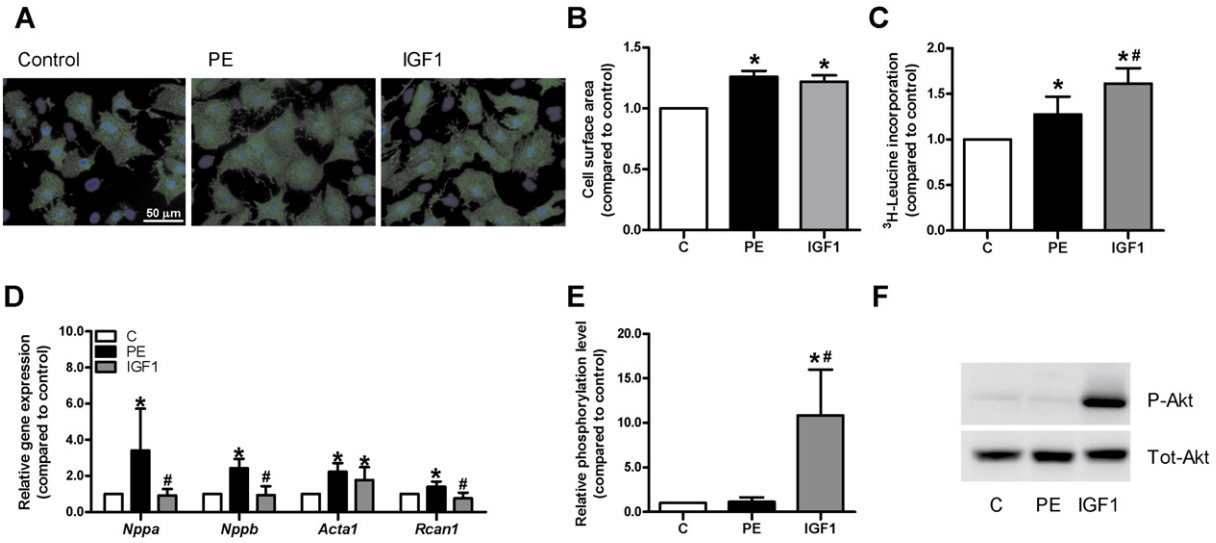

Fig. 1. Stimulation of NRVCs with PE or IGF1 induced hypertrophy. NRVCs were stimulated with PE or IGF1 for 24 h and hypertrophic responses were measured. Cell size was determined by staining with the sarcomeric cardiomyocyte specific marker α-actinin (green) and nuclei were counterstained with DAPI (blue). Representative images are shown (A). Quantification of cell surface area of PE or IGF1 stimulated NRVCs relative to control NRVCs (N = 3) (B). Protein synthesis was determined using ^{3}H-leucine incorporation (N = 11) (C). mRNA expression levels of the hypertrophic markers *Nppa*, *Nppb*, *Rcan1* and *Acta1* were determined using qRT-PCR (N = 6–8) (D). Protein expression levels of phosphorylated Akt and total Akt were determined by Western blot (N = 7) (E). Representative Western blot images are shown (F). All graphs depict means and SD, *P < 0.05 compared to control; #P < 0.05 compared to PE stimulated NRVCs. *Nppa*, atrial natriuretic peptide; *Nppb*, brain natriuretic peptide; *Rcan1*, regulator of calcineurin; *Acta1*, actin alpha1 skeletal muscle.

Nppa (*Anp*) and *Nppb* (*Bnp*) were significantly up-regulated in PE stimulated NRVCs (Fig. 1D), but expression did not change upon IGF1 treatment. *Acta1* was up-regulated upon stimulation with both stimuli and probably indicates a general response of the cardiomyocytes to hypertrophic stimulation (Fig. 1D). Whereas IGF1 strongly stimulated AKT phosphorylation (Fig. 1E and F), PE stimulated *Rcan1* expression, a marker for calcineurin activation. These results demonstrate that NRVCs show similar growth response upon PE and IGF1 stimulation,

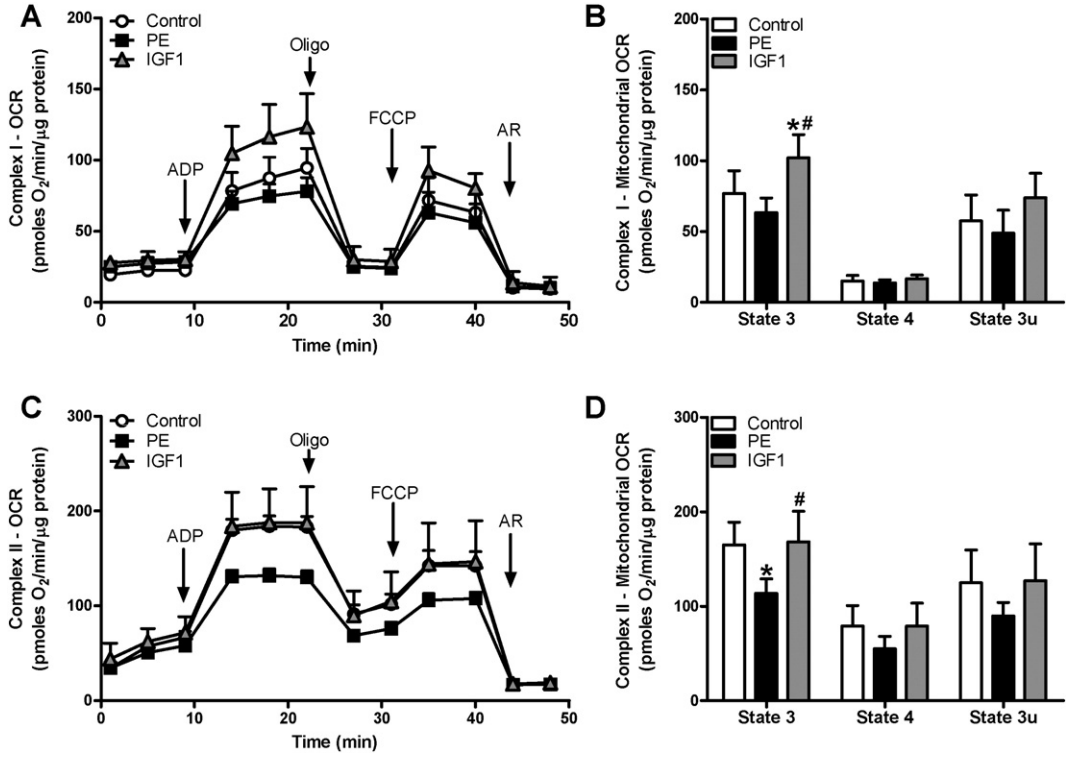

Fig. 2. Complex II dependent OCR is decreased after PE stimulation whereas IGF1 stimulation increased complex I dependent OCR. Total mitochondrial complex specific OCR was analyzed by permeabilizing NRVCs before measuring the OCR using a Seahorse XF24 Extracellular Flux Analyzer. Substrates were included in the buffer and basal respiration was measured. Sequential addition of ADP, oligomycin, FCCP and antimycin/rotenone (AR) is indicated in the graph. Parameters of complex specific mitochondrial respiration were calculated, after the subtraction of OCR measured after A/R resulting in mitochondrial specific OCR. State 3 is the OCR after the addition of ADP indicating the maximal coupled respiration. State 4 is the OCR after the addition of oligomycin, indicating the ATP-independent respiration. State 4u is induced after the addition of FCCP. Complex I dependent OCR was measured using pyruvate and malate as substrates (N = 6) (A)–(B). Complex II dependent OCR was measured using succinate as substrates and rotenone to inhibit complex I (N = 6) (C)–(D). All graphs depict means and SD, *P < 0.05 compared to control; #P < 0.05 compared to PE stimulated NRVCs.

but that the underlying hypertrophic pathways are not identical, reflecting the in vivo pathological and physiological differences.

3.2. PE stimulation decreased complex II activity, whereas IGF1 increased complex I activity

The general perception is that mitochondrial function declines in pathological cardiac hypertrophy, whereas it improves in physiological hypertrophy [10,11,25,26]. To investigate whether this could also be observed in NRVCs in vitro, the mitochondrial complex I and II dependent respiration in permeabilized NRVCs was determined using the Seahorse flux analyzer. Either malate/pyruvate was used as a substrate for complex I or succinate/rotenone for complex II. As shown in Fig. 2A and B, an increase in complex I dependent oxygen consumption rate (OCR) was observed after stimulation with IGF1, although only state 3 was significantly increased. No increase in complex I dependent OCR was observed after PE stimulation, rather a trend of lower complex I dependent OCR was shown. No differences in complex II dependent OCR were observed after stimulation with IGF1. Stimulation with PE resulted, however, in a significant diminishment of state 3 activity. Also state 4 and state 3u activities appeared lower after PE stimulation, albeit not significant (Fig. 2C and D). Thus, a specific pathological or physiological stimulus can, respectively, decrease and enhance specific mitochondrial complex activities in vitro.

3.3. NRVCs stimulated with PE, but not IGF1, have increased cellular mitochondrial respiration

The Seahorse flux analyzer provides the unique opportunity to measure mitochondrial OCR also in intact NRVCs. Fig. 3A and B shows the cellular OCR in control, PE and IGF1 stimulated NRVCs as determined in intact NRVCs using glucose as a substrate. Interestingly, cellular OCR was significantly higher in PE stimulated NRVCs, as compared to control and IGF1 stimulated NRVCs (Fig. 3A). Also after correction for non-mitochondrial OCR (total cellular OCR − A/R insensitive OCR), the mitochondrial specific OCR after stimulation with PE showed a significant increase of 2 fold as compared with control NRVCs (Fig. 3B). Addition of the ATP synthase inhibitor oligomycin revealed that the ATP-linked (oligomycin dependent) OCR was 3.5 fold higher in PE stimulated NRVCs. Maximal respiration induced by the addition of the uncoupler FCCP was also clearly increased and this trend was observed in all our experiments (Figs. 3, 8, Supplemental Figs. 1, 5), albeit not always significant. The latter is probably a power issue. No differences in mitochondrial respiration were observed in IGF1 stimulated NRVCs, indicating that increased OCR is not a prerequisite for hypertrophy development (Fig. 3B). Similar results were obtained using pyruvate as a substrate, indicating that these findings are not a result of changes in glycolysis (Supplemental Fig. 1). These data show that changes in complex activities do not necessarily reflect the mitochondrial fluxes in intact NRVCs.

3.4. Changes in mitochondrial respiration are not due to mitochondrial biogenesis

Altered mitochondrial biogenesis could explain the observed differences in the cellular mitochondrial respiration. To exclude mitochondrial biogenesis as a causal factor underlying these observed mitochondrial effects several parameters were investigated. Protein expression of the different complexes of the ETC was not altered in PE and IGF1 stimulated NRVCs, as shown with an OXPHOS Western blot (Fig. 4A and B). Also the ratio between mtDNA and nDNA, an established measurement of mitochondrial biogenesis, was similar between control, PE and IGF1 stimulated NRVCs (Fig. 4C). In addition, citrate synthase activity as an independent measurement of mitochondrial biogenesis was unaltered (Fig. 4D). This indicates that the observed changes in mitochondrial respiration were not mediated by increased mitochondrial biogenesis or increased levels of ETC proteins.

3.5. Changed mitochondrial localization in PE treated NRVCs

Although mitochondrial activity has been the main focus in cardiac energetics for many years, also mitochondrial dynamics and localization have increasingly gained interest in the cardiac field. Abnormalities have been described to affect mitochondrial function [27,28]. We stained NRVCs with an antibody against the mitochondrial outer membrane protein TOM20 [29]. Microscopic inspection revealed a strong perinuclear staining in control and IGF1 stimulated NRVCs, whereas PE stimulated NRVCs showed a more dispersed and cytoplasmic mitochondrial staining (Fig. 5A). This effect in PE treated cells was not simply a reflection of increased cell size, since both PE and IGF1 stimulated cells increased equally in size. Quantification of the ratio of perinuclear versus peripheral staining intensity confirmed a high intensity around the nucleus in control and even more in IGF1 stimulated NRVCs. This ratio was significantly lower in PE stimulated cells (Fig. 5B). Furthermore, counting the number of NRVCs with a low perinuclear/peripheral staining ratio (<3.0) confirmed this peripheral localization in PE stimulated NRVCs (Fig. 5C). Thus, PE, but not IGF1, stimulates peripheral mitochondrial localization in NRVCs.

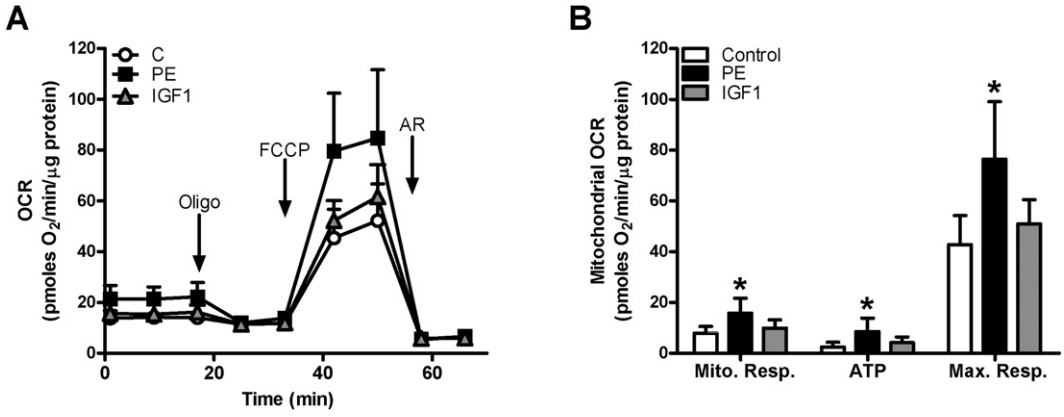

Fig. 3. Mitochondrial respiration in intact NRVCs is increased after stimulation with PE. Total cellular OCR was measured using a Seahorse XF24 Extracellular Flux Analyzer, with sequential addition of the ATP synthase inhibitor oligomycin, the uncoupling agent FCCP and mitochondrial respiration inhibitors antimycin A/rotenone (AR) as depicted in the graph (A). Mitochondrial specific OCR values were obtained by subtracting OCR values after the addition of AR from total OCR resulting in mitochondrial respiration, maximal and ATP-linked OCR. Corrected oxygen consumption data of the first 3 measurements were averaged to yield the mitochondrial respiration. The ATP-linked OCR, defined as oligomycin-sensitive OCR, was calculated. Maximal respiration was induced by FCCP (N = 5) (B). All graphs depict means and SD, *P < 0.05 compared to control.

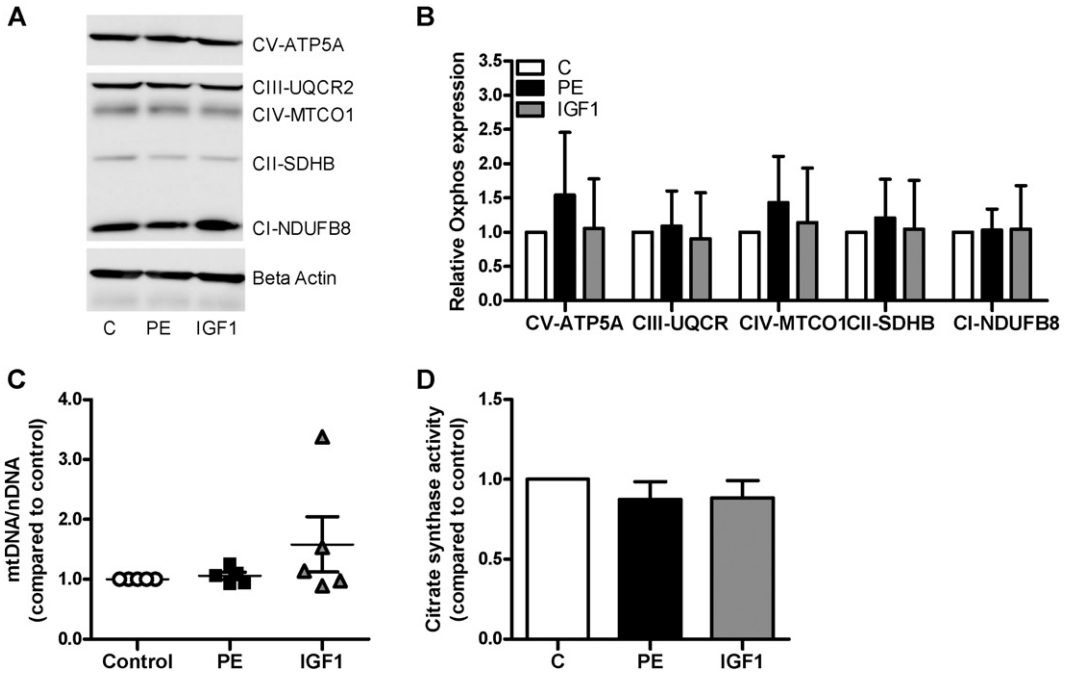

Fig. 4. Increased mitochondrial respiration is not due to mitochondrial biogenesis. Several independent measurements of mitochondrial biogenesis were assessed in PE and IGF1 stimulated NRVCs. Total cellular protein was blotted and incubated with specific OXPHOS antibody to assess protein expression levels of the different complexes of the ETC. A representative Western blot is shown (A) and the expression of the separate complexes was quantified (N = 11) (B). RT-PCR analysis was used to compare the amount of mtDNA with nDNA (N = 5) (C). Whole cell citrate synthase activity was measured using an enzyme assay kit (N = 5) (D). All graphs depict means and SD.

3.6. Gene array analysis reveals upregulation of Kif5b in PE treated NRVCs

Gene expression changes could potentially reveal targets that explain the observed differences. A gene array analysis was therefore performed with RNA from control, PE and IGF1 stimulated NRVCs. Using a FDR of 10%, we identified >300 genes that were differentially expressed in PE stimulated NRVCs, compared to almost 1200 genes in IGF1 stimulated NRVCs. Of these genes at least 4.9% of both the PE and IGF1 group translated into proteins that are localized to the mitochondria, based on available proteomic data (Fig. 6A) [30]. This mitochondrial set was further explored using DAVID to categorize genes into biological processes (Fig. 6B). No specific functionally related groups

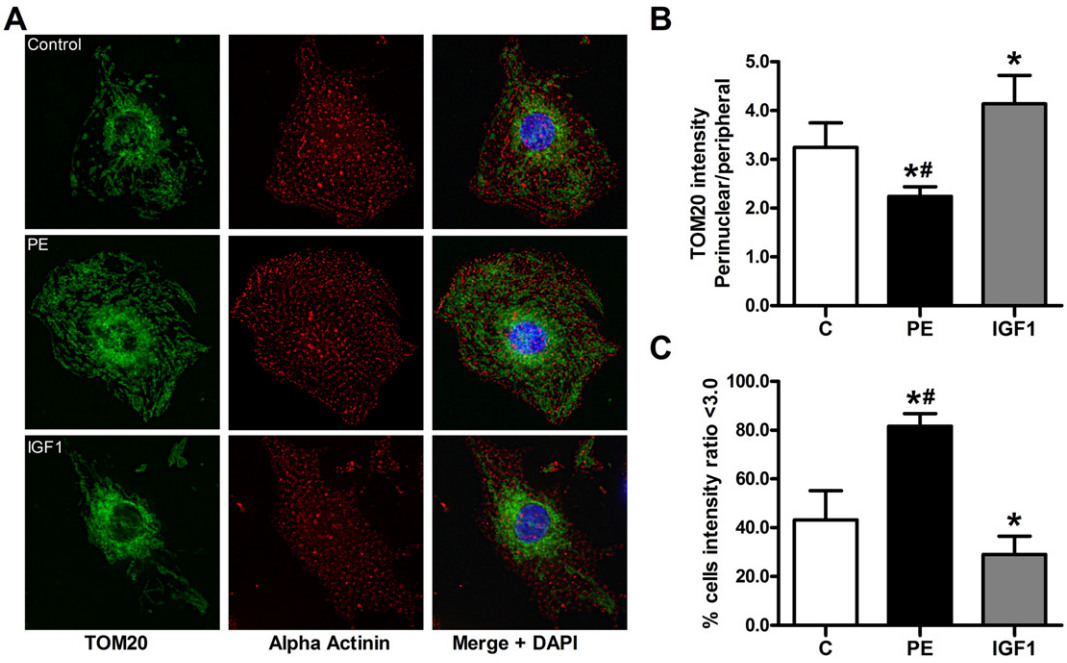

Fig. 5. Mitochondria in PE stimulated NRVCs are dispersed throughout the cytosol. Mitochondrial localization was visualized by staining NRVCs with anti-TOM20 antibody (green). NRVCs were stained with specific sarcomeric α-actinin (red) and nuclei were counterstained with DAPI (blue). Representative pictures are shown (A). Quantification of the intensity of perinuclear localized mitochondrial staining as compared to peripheral cytoplasmic mitochondrial staining (N = 6) (B). Quantification of the percentage of NRVCs with a perinuclear versus peripheral mitochondrial fluorescence intensity ratio lower than 3 (N = 6) (C). All graphs depict means and SD, *P < 0.05 compared to control. #P < 0.05 compared to IGF1 stimulated NRVCs.

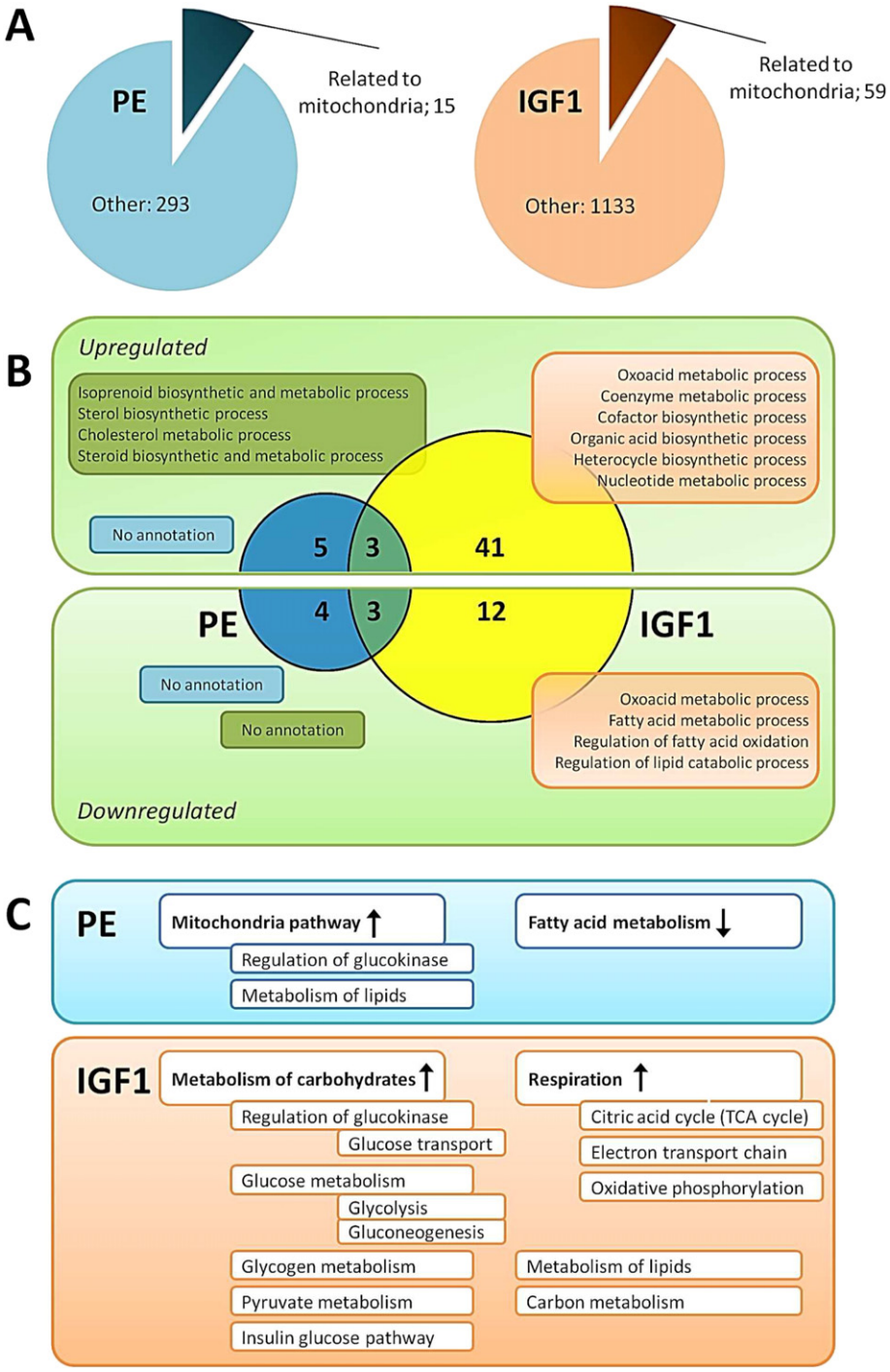

Fig. 6. Analysis of gene expression arrays of control versus PE and IGF1 stimulated NRVCs. Gene expression was analyzed using Affymetrics gene expression arrays. RNA of control, PE and IGF1 stimulated cells was isolated and used for expression analysis (A). Expression of genes encoding mitochondrial proteins was analyzed. Using a FDR < 10% revealed a number of genes that were differentially expressed in NRVCs upon stimulation with PE or IGF1 (A). Analysis of the significantly regulated genes related to the mitochondria. The number of differentially expressed genes related to the mitochondria compared to control in PE-treated NRVCs (blue) and IGF1-treated NRVCs (yellow) is depicted in circles, common genes are shown in green. The biological processes (DAVID) to which these genes are related are shown in respective boxes (B). A simplified scheme of gene sets that were significantly regulated upon stimulation with PE or IGF1 (C).

of genes were found in the PE stimulated NRVCs (Fig. 6B) but within the 9 specific PE controlled genes, we identified upregulation of *Bcl2* (anti-apoptotic) and downregulation of *Htra2* (apoptotic), which is in line with a previously described link between PE and protection against cardiomyocyte apoptosis [31,32]. Only 6 genes were shared between PE and IGF1 stimulated NRVCs, identifying enriched biological pathways in isoprenoid, sterol and cholesterol biosynthetic and metabolic processes (Fig. 6B). In IGF1 stimulated NRVCs more mitochondrial related genes were differentially expressed. For the IGF1 gene set functional annotation revealed enrichment in several metabolic and biosynthetic processes including oxoacid, coenzyme, cofactor, organic acid, heterocycle, nucleotide and fatty acid metabolic and biosynthetic processes. No major changes in specific ETC related gene expression were observed (Fig. 6B and Supplemental data set).

Whole gene set enrichment analysis, which allows detection of changes in gene sets not depending on significant changed expression

of individual genes, did however, show significant differences. A schematic and simplified overview of gene sets related to metabolism is shown in Fig. 6C. A number of changes related to metabolism in IGF1 stimulated NRVCs were observed, including the TCA cycle, the ETC and the OXPHOS pathways. In PE stimulated NRVCs less changes in specific gene sets were found, including fatty acid metabolism (Fig. 6C). Thus, changes in the expression of genes encoding mitochondrial localized proteins are small in these 24 h PE and IGF1 stimulated NRVCs.

3.7. The kinesin motor protein KIF5B is specifically upregulated in PE treated cells

Based on our localization data, we also investigated genes potentially involved in mitochondrial dynamics and localization. We did not observe gene expression differences in genes involved in mitochondrial fission/fusion and also protein levels and dynamic localization of two of these proteins, dynamin-like protein (Drp1) and mitofusin (Mfn1/2) were not altered (Supplemental Fig. 2). We did, however, identify several kinesin and dynein motor proteins in our gene array that were differentially expressed between the different conditions (Fig. 7A). Most interestingly, *Kif5b* showed the highest expression and was upregulated under PE stimulatory conditions only (1.6 fold increase). Moreover, we could confirm that KIF5B protein levels were similarly increased in PE stimulated cells only (Fig. 7B). KIF5B has previously been shown to affect localization of the mitochondria in tumor cell lines [33]. Also in in vivo hypertrophic conditions disturbed morphology and mitochondrial localization have been reported [28,34–38]. We therefore analyzed whether *Kif5b* gene expression was altered in mice with

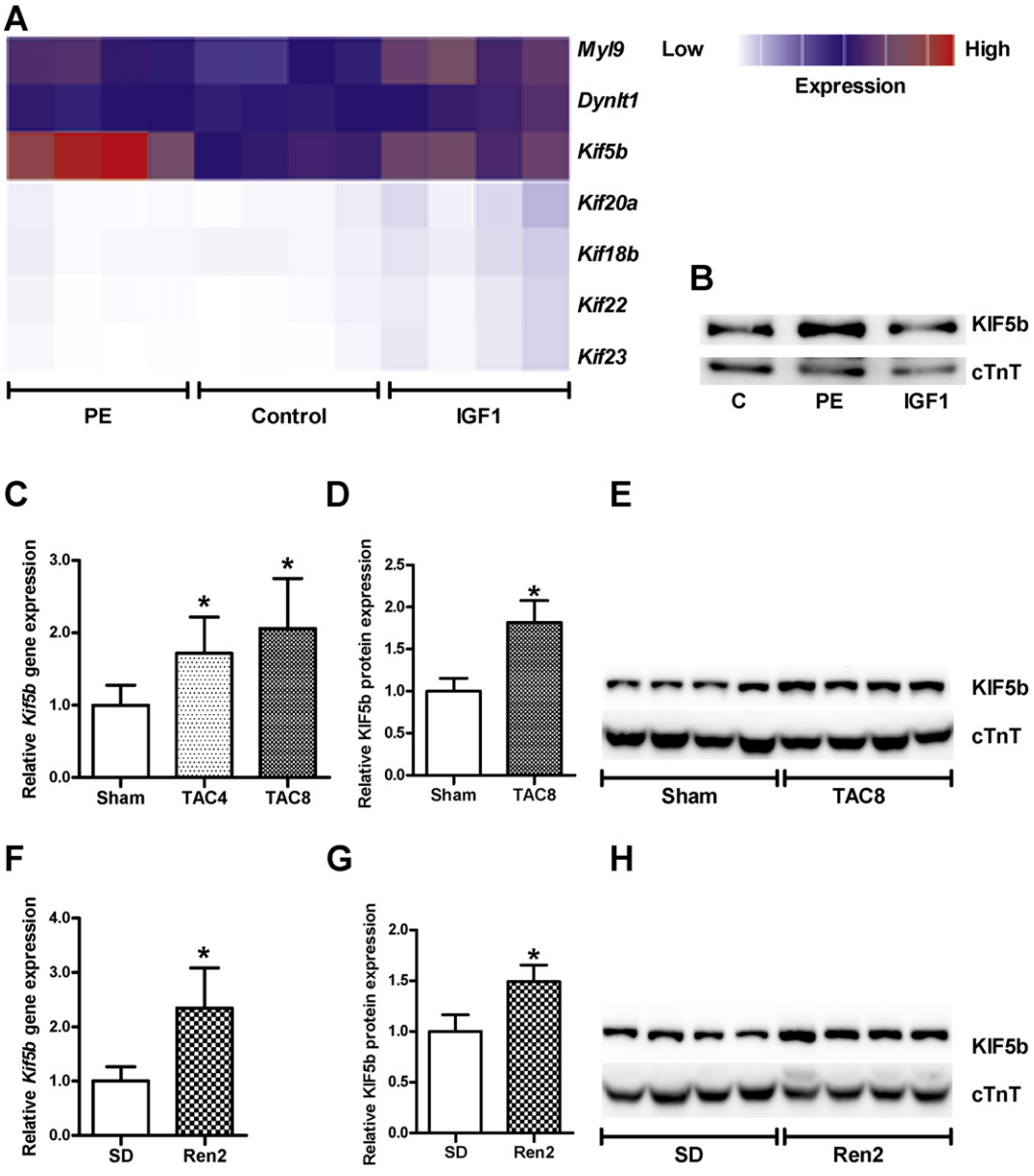

Fig. 7. Increased KIF5B expression in animal models of pathological hypertrophy. Based on gene expression array data described in Fig. 6, differentially expressed genes encoding motor proteins (FDR < 10%) were identified in the PE stimulated or IGF1 stimulated NRVCs. A heat-map of these genes is shown (A). To confirm expression in animal models of hypertrophy *Kif5b* gene expression was measured by quantitative RT-PCR in cardiac tissue. *Kif5b* expression in mice after 4 and 8 weeks TAC surgery (N = 7–12). Expression of Kif5b protein levels after 36 h PE stimulation was evaluated by Western blotting and a representative blot from three independent experiments is shown (B). To confirm expression in animal cardiac hypertrophy models, *Kif5b* gene and protein expression were determined by quantitative RT-PCR and Western blotting, respectively. Cardiac *Kif5b* gene expression in mice after 4 and 8 weeks TAC surgery (N = 7–12) (C). Quantification of KIF5B protein expression in mice after 8 weeks TAC surgery (N = 6) (D) and representative Western blot (E). *Kif5b* gene expression in transgenic Ren2 rats (N = 8–9) (F). KIF5B protein expression in transgenic Ren2 rats (N = 6) (G) and representative Western blot (H). All graphs depict means and SD, *P < 0.05 as compared to control.

cardiac hypertrophy generated by transverse aortic constriction (TAC) and in hypertensive transgenic Ren2 rats. *Kif5b* gene expression was indeed elevated in the animal models with pathological hypertrophy (Fig. 7C and D). Also in this case KIF5B protein levels paralleled the gene expression increases (Fig. 7C and D). We also like to note that we did not observe an increase in *Kif5b* gene expression in a physiological mouse hypertrophy model (Supplemental Fig. 3). Together these data suggests that KIF5B could control mitochondrial dynamic localization in cardiac tissue in response to pathological hypertrophic stimuli.

3.8. Depletion of KIF5B prevented mitochondrial dispersion and limited the respiratory increase

Silencing of *Kif5b* was performed to investigate whether KIF5B could be responsible for the changed mitochondrial localization in PE treated NRVCs. Transfection of specific siRNA's targeting *Kif5b* resulted approximately in a 75% decrease in *Kif5b* mRNA levels (Fig. 8A) and around 70% decrease in KIF5B protein levels (Fig. 8B). Interestingly, this fully prevented PE induced dispersion of the mitochondria as is

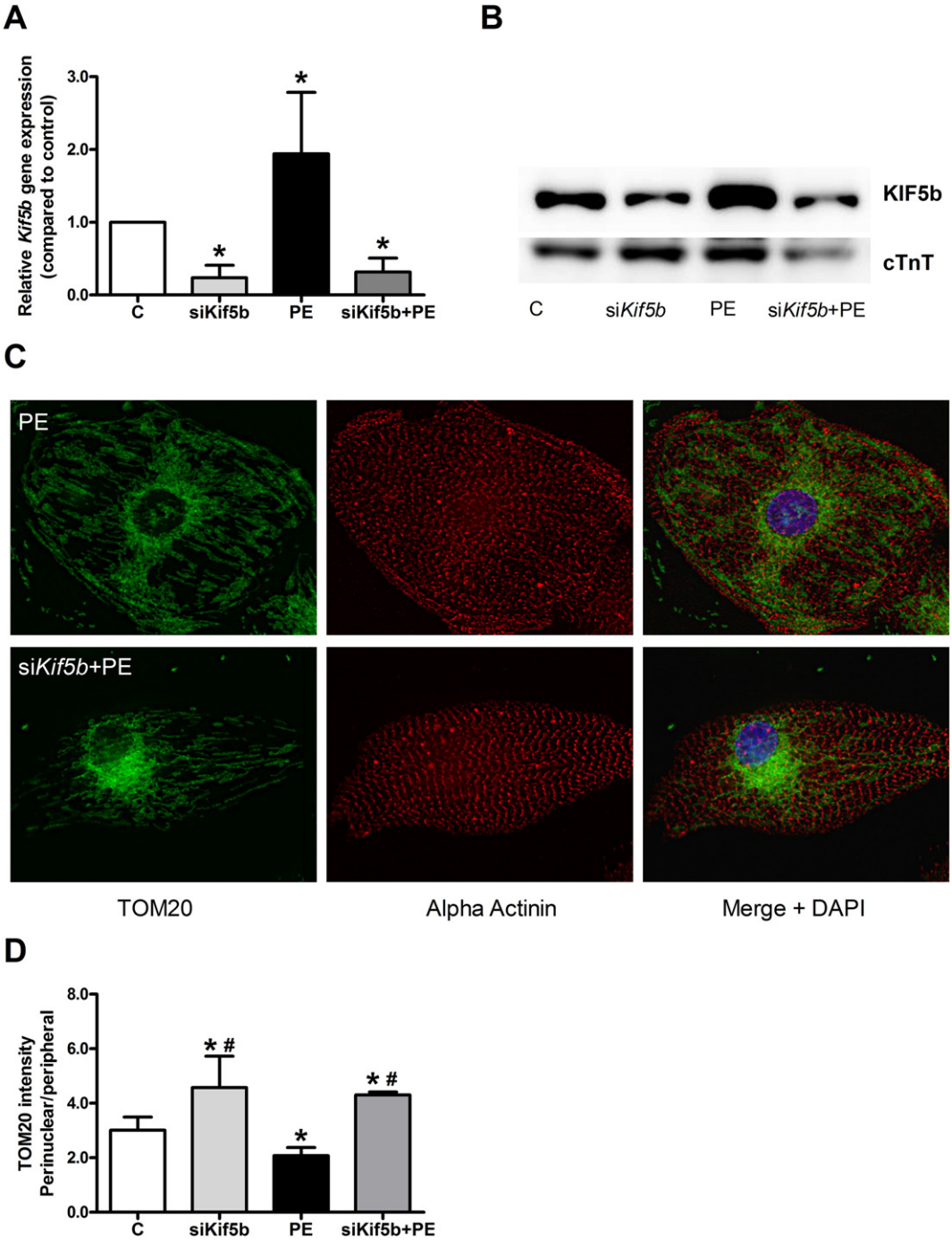

Fig. 8. *Kif5b* silencing in NRVCs affects mitochondrial localization. *Kif5b* was silenced in NRVCs for 72 h. *Kif5b* mRNA levels were measured by quantitative RT-PCR in control cells and PE stimulated NRVCs (N = 6) (A). Protein expression levels were measured by Western blot in control and PE stimulated NRVCs and a representative blot from three independent experiments is shown (B). Mitochondrial localization is visualized by staining mitochondria with anti-TOM20 antibody (green). Cardiomyocytes were stained with cardiac specific sarcomeric α-actinin (red) and nuclei were counterstained with DAPI (blue). Representative images are shown (B). Quantification of the ratio in intensity of perinuclear and peripheral cytoplasmic TOM20 signal (N = 4) (D).

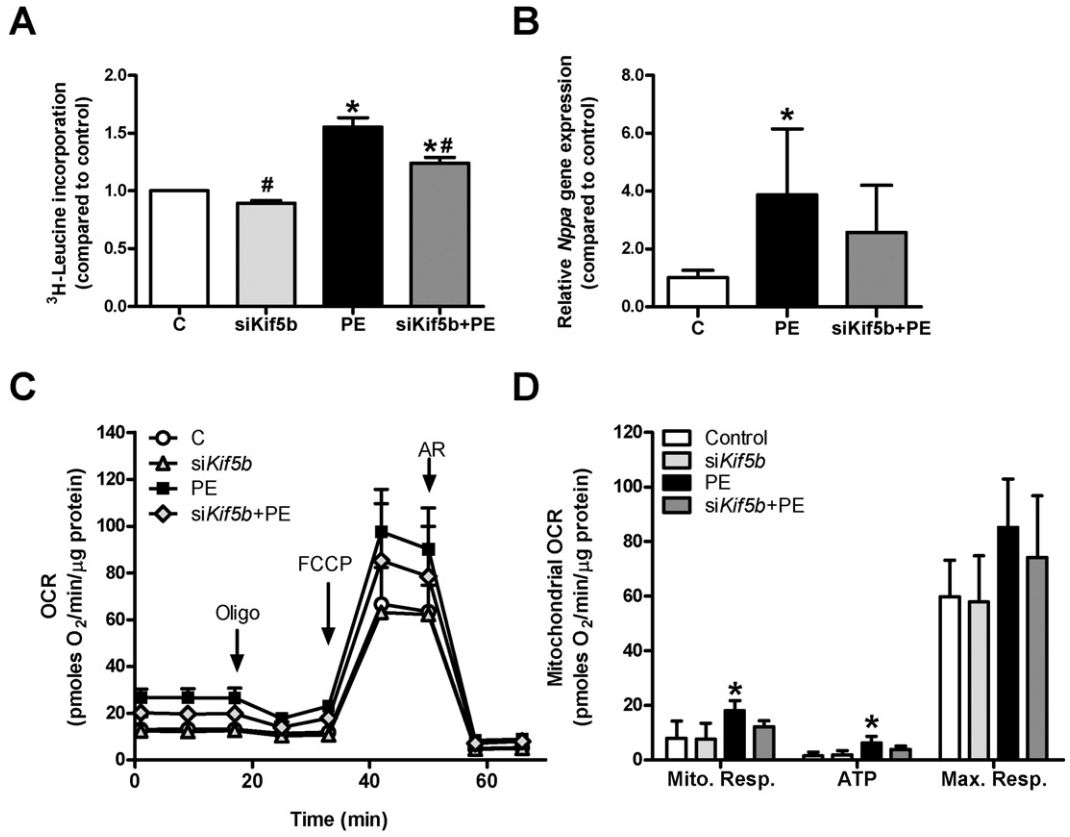

Fig. 9. *Kif5b* silencing partially reverses PE induced effects on mitochondrial dependent cellular respiration and hypertrophy. Effects of silencing of *Kif5b* on PE induced cellular hypertrophy was measured using ^{3}H-leucine incorporation (N = 3) (A). mRNA expression levels of the hypertrophic markers *Nppa*were determined using qRT-PCR (N = 3) (B). Total cellular OCR using pyruvate as a substrate was measured with sequential additions of the ATP synthase inhibitor oligomycin, the uncoupling agent FCCP and mitochondrial respiration inhibitors antimycin A/rotenone (AR) as depicted in the graph (C). Mitochondrial specific OCR values, mitochondrial respiration, ATP-linked OCR and maximal respiration, were determined by correcting the total OCR values for OCR values after the addition of AR. Corrected oxygen consumption data of the first 3 measurements were averaged to yield the mitochondrial respiration. The ATP-linked OCR, defined as oligomycin-sensitive OCR, was calculated. Maximal respiration was induced by FCCP (N = 4) (D). All graphs depict means and SD, *P < 0.05 compared to control.

shown by the intensity of TOM20 staining (Fig. 8C and D). Thus, also in cardiomyocytes, Kif5b is involved in mitochondrial transport. We also investigated whether this changed localization would affect cellular respiration and hypertrophy. Silencing of *Kif5b* attenuated PE induced 3H-leucine incorporation, but did not prevent it (Fig. 9A) and a similar effect was observed on cell size (1.34 ± 0.15 versus 1.21 ± 0.12 fold increase for PE and siKif5B + PE, respectively). Pathological gene expression was, however, not attenuated by KIF5B silencing (Fig. 9B and Supplemental Fig. 4). Also respiration was investigated, and, since it has been reported that the scaffold protein Daxx together with KIF5B controls insulin mediated translocation of the glucose transporter Glut4 in adipose cells [39], we performed these experiments with pyruvate as a carbon source. In control cells *Kif5b* silencing did not show a significant effect on respiration, but in PE treated NRVCs silencing of *Kif5b* showed a partial diminishment (Fig. 9C and D). Similar results were observed when glucose was used as a substrate instead of pyruvate, indicating that the observed effects were carbon source and hence transporter independent (Supplemental Fig. 5). Thus, mitochondrial relocalization by KIF5B affects mitochondrial dependent cellular respiration and attenuates phenylephrine induced hypertrophy.

4. Discussion

Hypertrophic stimuli induce cardiomyocyte growth, but the biochemical and molecular alterations are clearly different between various hypertrophic stimuli. Here we show that this is also true for mitochondrial localization and function in vitro. Using neonatal cardiomyocyte cultures, we were able to determine the effects of specific hypertrophic stimuli on mitochondrial localization. Interestingly, stimulation of NRVCs with PE resulted in an altered mitochondrial OCR and mitochondrial localization within 24 h. *Kif5b* was identified as a pathological hypertrophy specific gene and was responsible for the changes in mitochondrial localization. Altered mitochondrial morphology and distribution are hallmarks of heart failure [37,38] and we could show that also in pathological hypertrophy animal models, KIF5B expression was upregulated.

Hypertrophic stimulation with PE or IGF1 resulted in the activation of different signal transduction pathways. Moreover, in agreement with others, only PE stimulation resulted in the expression of the fetal gene program, a pathological hypertrophy characteristic. Here we showed that these different stimuli also have direct, but distinct effects on mitochondrial function and localization. Measurements of the activities of mitochondrial complexes I and II revealed the opposite effect in PE and IGF1 stimulated NRVCs. Whereas complex II and to a lesser extend complex I dependent activity (state 3) were declined in PE stimulated NRVCs, complex I dependent activity (state 3) was increased in IGF1 treated NRVCs. Also in hypertrophic HF samples a decline in activities of different complexes has been observed, but there is limited consensus which complex activities are altered [40–42]. This is probably related to the differences in the etiology and severity of disease and it has been proven difficult to uncover the processes that underlie these changed activities. To our knowledge, we now show for the first time that complex I and II dependent activities can be modulated by specific hypertrophic stimuli in vitro and this may provide an opportunity to study these processes in more detail in an isolated cellular system. This also suggests that changes in mitochondrial function can

already arise early during hypertrophy development and are not necessarily a late stage HF phenomenon, which is in agreement with others [43].

Despite decreased complex activities, mitochondrial respiration was strongly increased in PE stimulated NRVCs. In contrast no changes in mitochondrial respiration were observed in IGF1 stimulated NRVCs. Thus, changes in mitochondrial complex activities do not necessarily reflect mitochondrial fluxes in intact NRVCs and caution is required when results from isolated mitochondria are extrapolated to the whole cell or organ. It has been proposed that in the compensated stage of hypertrophy, respiratory flux may first increase resulting in a gradual decline at later stages [11]. Our increase in flux in PE stimulated NRVCs may support this idea and suggest that the PE condition with increased OCR is more comparable to early stages of cardiac pathological hypertrophy. These results show that no simple relation exists between mitochondrial function and hypertrophy development.

Within the investigated time frame (24 h) no significant changes in mitochondrial biogenesis or levels of OXPHOS proteins were observed with the two different hypertrophic stimuli. Also no significant changes in the expression of genes of the ETC and OXPHOS were identified. However, we do like to note that when whole gene set analysis was performed, ETC complex expression was significantly upregulated in IGF1 stimulated NRVCs. These minor differences could, however, not be identified at the protein level, and probably the 24 h stimulation is too short to induce IGF1 mediated mitochondrial biogenesis in NRVCs. The changes in complex activities are therefore likely mediated by posttranslational processes, like phosphorylation, succinylation and acetylation [44,45] and complex or supercomplex assembly [46]. In contrast to our in vitro data, a number of studies have shown that mitochondrial gene expression is altered in cardiac HF samples. These studies have, however, predominantly been performed on end-stage HF cardiac tissue [47,48]. A recent study, with a focus on earlier stages of HF, with less severe cardiac remodeling showed the absence of transcriptional changes in OXPHOS and ETC genes [5], which is in line with our in vitro data.

IGF1 signaling is essential for mitochondrial biogenesis during physiological hypertrophy stimulation in mice [49]. In a transgenic IGF1 overexpressing mouse model PGC-1 alpha expression and mitochondrial protein levels were, however, not increased, but high fat diet induced repression of mitochondrial biogenesis was prevented [50]. Thus, IGF1 alone appears not sufficient for induction of mitochondrial biogenesis. Also in this study no mitochondrial biogenesis was observed upon IGF1 stimulation and gene expression of mitochondrial gene sets was only slightly elevated. Mitochondrial biogenesis is thus not required for the development of physiological hypertrophy.

Mitochondria in PE treated NRVCs showed a different localization pattern and we identified KIF5B, a motor protein of the kinesin family reported to control mitochondrial localization and function, to be upregulated under pathological hypertrophy. Moreover, depletion of KIF5B confirmed that this protein is required for the changed localization in PE treated NRVCs. Depletion of KIF5B also resulted in diminished hypertrophy development after PE stimulation, but could not prevent pathological gene expression. Thus, KIF5B contributes to pathological growth, but is not essential for the pathological response. Although we focused here on dynamic mitochondrial localization, also effects on other mitochondrial dynamics, namely fission and fusion have been reported. Whereas Javadov et al. [51] reported altered expression of dynamin-like protein (Drp1) and mitofusin (Mfn1/2), Pennanen et al. [35] did not observe differences in the expression of these proteins after hypertrophic stimulation of neonatal cardiomyocytes. Nevertheless they reported that norepinephrine (NE) can stimulate mitochondrial fission by increasing the localization of Drp1 to the mitochondria [35]. In our PE stimulation we did not observe changes in Drp1 and Mfn1 gene and protein expression in agreement with Pennanen et al. [35], but did not also observe mitochondrial redistribution of Drp1 or Mfn1. The use of PE instead of NE could potentially explain this difference, and we do not like to exclude potential alterations in mitochondrial morphology, but the altered localization makes this difficult to analyze. Together these results show that pathological conditions can alter mitochondrial localization and potentially morphology and thereby affecting mitochondrial function. Also in heart failure patients and in animal heart failure models changed morphology and localization of the mitochondria have been reported [28,37,38] and with the identification of a potential molecular mechanism this now warrants further investigations. In the adult cardiomyocyte the situation is, however, more complex with two different types of the mitochondria, subsarcolemmal (SS) and intermyofibrillar (IFM) [52]. It is likely that other factors next to KIF5B play a role in the proper localization of these distinct mitochondrial populations.

Some study limitations have to be taken into account. Although neonatal rat cardiomyocytes are an established in vitro hypertrophy model, these results cannot be directly translated to the adult heart. The model has, however, a major advantage in that it allows to investigate single stimuli independent of other contributing factors and that it is feasible to perform mitochondrial OCR measurements in intact NRVCs. Although we have investigated the levels of some mitochondrial complex proteins, to exclude changes in biogenesis, we have not investigated complex formation or post-translational modifications. Considering our results elaborate mass spectrometry analysis might be an interesting next step.

In conclusion, we provide for the first time an in vitro model of mitochondrial dysfunction and changed dynamic localization in pathological and physiological cardiac hypertrophy. We identify KIF5B as a gene that is upregulated exclusively in pathological hypertrophy with a role in mitochondrial localization and function.

Supplementary data to this article can be found online at http://dx.doi.org/10.1016/j.yjmcc.2016.04.005.

Disclosures

The authors declare no conflict of interest.

Financial support

R.A de Boer is supported by the Innovational Research Incentives Scheme program of the Netherlands Organisation for Scientific Research [Vidi grant 917.13.350].

Acknowledgments

We like to thank Sarah Meijer, Reinier Bron and Louise van Wijk for help with Western blotting, microscopy, cell counting and RNA analysis. We like to thank Moshin Kahn for help with generating heat-maps in "R". We like to thank Laura Meems for supplying us with RNA of animal experiments.

References

[1] S.P. Barry, S.M. Davidson, P.A. Townsend, Molecular regulation of cardiac hypertrophy, Int. J. Biochem. Cell Biol. 40 (2008) 2023–2039.
[2] N. Frey, H.A. Katus, E.N. Olson, J.A. Hill, Hypertrophy of the heart: a new therapeutic target? Circulation 109 (2004) 1580–1589.
[3] B.C. Bernardo, K.L. Weeks, L. Pretorius, J.R. McMullen, Molecular distinction between physiological and pathological cardiac hypertrophy: experimental findings and therapeutic strategies, Pharmacol. Ther. 128 (2010) 191–227.
[4] R.A. De Boer, Y.M. Pinto, D.J. Van Veldhuisen, The imbalance between oxygen demand and supply as a potential mechanism in the pathophysiology of heart failure: the role of microvascular growth and abnormalities, Microcirculation 10 (2003) 113–126.
[5] L. Lai, T.C. Leone, M.P. Keller, O.J. Martin, A.T. Broman, J. Nigro, et al., Energy metabolic reprogramming in the hypertrophied and early stage failing heart: a multisystems approach, Circ. Heart Fail. 7 (2014) 1022–1031.
[6] P.C. Kienesberger, T. Pulinilkunnil, J. Nagendran, J.R. Dyck, Myocardial triacylglycerol metabolism, J. Mol. Cell. Cardiol. 55 (2013) 101–110.
[7] S.C. Kolwicz Jr., R. Tian, Glucose metabolism and cardiac hypertrophy, Cardiovasc. Res. 90 (2011) 194–201.

[8] J.J. Lehman, D.P. Kelly, Gene regulatory mechanisms governing energy metabolism during cardiac hypertrophic growth, Heart Fail. Rev. 7 (2002) 175–185.
[9] B.T. O'Neill, J. Kim, A.R. Wende, H.A. Theobald, J. Tuinei, J. Buchanan, et al., A conserved role for phosphatidylinositol 3-kinase but not Akt signaling in mitochondrial adaptations that accompany physiological cardiac hypertrophy, Cell Metab. 6 (2007) 294–306.
[10] E.D. Abel, T. Doenst, Mitochondrial adaptations to physiological vs. pathological cardiac hypertrophy, Cardiovasc. Res. 90 (2011) 234–242.
[11] M.G. Rosca, B. Tandler, C.L. Hoppel, Mitochondria in cardiac hypertrophy and heart failure, J. Mol. Cell. Cardiol. 55 (2013) 31–41.
[12] B. Lu, H. Mahmud, A.H. Maass, B. Yu, W.H. van Gilst, R.A. de Boer, et al., The Plk1 inhibitor BI 2536 temporarily arrests primary cardiac fibroblasts in mitosis and generates aneuploidy in vitro, PLoS One 5 (2010), e12963.
[13] B. Lu, H. Yu, M. Zwartbol, W.P. Ruifrok, W.H. van Gilst, R.A. de Boer, et al., Identification of hypertrophy- and heart failure-associated genes by combining in vitro and in vivo models, Physiol. Genomics 44 (2012) 443–454.
[14] R.A. de Boer, S. Pokharel, M. Flesch, D.A. van Kampen, A.J. Suurmeijer, F. Boomsma, et al., Extracellular signal regulated kinase and SMAD signaling both mediate the angiotensin II driven progression towards overt heart failure in homozygous TGR(mRen2)27, J. Mol. Med. 82 (2004) 678–687.
[15] O.J. Muller, M. Lange, H. Rattunde, H.P. Lorenzen, M. Muller, N. Frey, et al., Transgenic rat hearts overexpressing SERCA2a show improved contractility under baseline conditions and pressure overload, Cardiovasc. Res. 59 (2003) 380–389.
[16] J.K. Salabei, A.A. Gibb, B.G. Hill, Comprehensive measurement of respiratory activity in permeabilized cells using extracellular flux analysis, Nat. Protoc. 9 (2014) 421–438.
[17] W. Tigchelaar, H. Yu, A.M. de Jong, W.H. van Gilst, P. van der Harst, B.D. Westenbrink, et al., Loss of mitochondrial exo/endonuclease EXOG affects mitochondrial respiration and induces ROS-mediated cardiomyocyte hypertrophy, Am. J. Physiol. Cell Physiol. 308 (2015) C155–C163.
[18] K. Lin, H. Kools, P.J. de Groot, A.K. Gavai, R.K. Basnet, F. Cheng, et al., MADMAX — management and analysis database for multiple ~omics experiments, J. Integr. Bioinform. 8 (2011) 160 (jib-2011-160).
[19] M.A. Sartor, C.R. Tomlinson, S.C. Wesselkamper, S. Sivaganesan, G.D. Leikauf, M. Medvedovic, Intensity-based hierarchical Bayes method improves testing for differentially expressed genes in microarray experiments, BMC Bioinf. 7 (2006) 538.
[20] J.D. Storey, R. Tibshirani, Statistical significance for genomewide studies, Proc. Natl. Acad. Sci. U. S. A. 100 (2003) 9440–9445.
[21] W. Huang da, B.T. Sherman, R.A. Lempicki, Systematic and integrative analysis of large gene lists using DAVID bioinformatics resources, Nat. Protoc. 4 (2009) 44–57.
[22] A. Subramanian, P. Tamayo, V.K. Mootha, S. Mukherjee, B.L. Ebert, M.A. Gillette, et al., Gene set enrichment analysis: a knowledge-based approach for interpreting genome-wide expression profiles, Proc. Natl. Acad. Sci. U. S. A. 102 (2005) 15545–15550.
[23] A.M. De Jong, I.C. Van Gelder, I. Vreeswijk-Baudoin, M.V. Cannon, W.H. Van Gilst, A.H. Maass, Atrial remodeling is directly related to end-diastolic left ventricular pressure in a mouse model of ventricular pressure overload, PLoS One 8 (2013), e72651.
[24] M.A. Lee, M. Bohm, M. Paul, M. Bader, U. Ganten, D. Ganten, Physiological characterization of the hypertensive transgenic rat TGR(mREN2)27, Am. J. Phys. 270 (1996) E919–E929.
[25] V.G. Sharov, A.V. Todor, N. Silverman, S. Goldstein, H.N. Sabbah, Abnormal mitochondrial respiration in failed human myocardium, J. Mol. Cell. Cardiol. 32 (2000) 2361–2367.
[26] C.C. Strom, M. Aplin, T. Ploug, T.E. Christoffersen, J. Langfort, M. Viese, et al., Expression profiling reveals differences in metabolic gene expression between exercise-induced cardiac effects and maladaptive cardiac hypertrophy, FEBS J. 272 (2005) 2684–2695.
[27] G.W. Dorn II, Mitochondrial dynamics in heart disease, Biochim. Biophys. Acta 2013 (1833) 233–241.
[28] G.W. Dorn II, Mitochondrial dynamism and heart disease: changing shape and shaping change, EMBO Mol. Med. 7 (2015) 865–877.
[29] M. Yano, M. Kanazawa, K. Terada, M. Takeya, N. Hoogenraad, M. Mori, Functional analysis of human mitochondrial receptor Tom20 for protein import into mitochondria, J. Biol. Chem. 273 (1998) 26844–26851.
[30] D.J. Pagliarini, S.E. Calvo, B. Chang, S.A. Sheth, S.B. Vafai, S.E. Ong, et al., A mitochondrial protein compendium elucidates complex I disease biology, Cell 134 (2008) 112–123.
[31] L.L. Yao, Y.G. Wang, X.J. Liu, Y. Zhou, N. Li, J. Liu, et al., Phenylephrine protects cardiomyocytes from starvation-induced apoptosis by increasing glyceraldehyde-3-phosphate dehydrogenase (GAPDH) activity, J. Cell. Physiol. 227 (2012) 3518–3527.
[32] H. Zhu, S. McElwee-Witmer, M. Perrone, K.L. Clark, A. Zilberstein, Phenylephrine protects neonatal rat cardiomyocytes from hypoxia and serum deprivation-induced apoptosis, Cell Death Differ. 7 (2000) 773–784.
[33] Y. Tanaka, Y. Kanai, Y. Okada, S. Nonaka, S. Takeda, A. Harada, et al., Targeted disruption of mouse conventional kinesin heavy chain, kif5B, results in abnormal perinuclear clustering of mitochondria, Cell 93 (1998) 1147–1158.
[34] L. Fang, X.L. Moore, X.M. Gao, A.M. Dart, Y.L. Lim, X.J. Du, Down-regulation of mitofusin-2 expression in cardiac hypertrophy in vitro and in vivo, Life Sci. 80 (2007) 2154–2160.
[35] C. Pennanen, V. Parra, C. Lopez-Crisosto, P.E. Morales, A. Del Campo, T. Gutierrez, et al., Mitochondrial fission is required for cardiomyocyte hypertrophy mediated by a Ca2+-calcineurin signaling pathway, J. Cell Sci. 127 (2014) 2659–2671.
[36] Y. Tang, C. Mi, J. Liu, F. Gao, J. Long, Compromised mitochondrial remodeling in compensatory hypertrophied myocardium of spontaneously hypertensive rat, Cardiovasc. Pathol. 23 (2014) 101–106.
[37] L. Chen, Q. Gong, J.P. Stice, A.A. Knowlton, Mitochondrial OPA1, apoptosis, and heart failure, Cardiovasc. Res. 84 (2009) 91–99.
[38] J. Schaper, R. Froede, S. Hein, A. Buck, H. Hashizume, B. Speiser, et al., Impairment of the myocardial ultrastructure and changes of the cytoskeleton in dilated cardiomyopathy, Circulation 83 (1991) 504–514.
[39] V.S. Lalioti, S. Vergarajauregui, Y. Tsuchiya, S. Hernandez-Tiedra, I.V. Sandoval, Daxx functions as a scaffold of a protein assembly constituted by GLUT4, JNK1 and KIF5B, J. Cell. Physiol. 218 (2009) 416–426.
[40] A.M. Cordero-Reyes, A.A. Gupte, K.A. Youker, M. Loebe, W.A. Hsueh, G. Torre-Amione, et al., Freshly isolated mitochondria from failing human hearts exhibit preserved respiratory function, J. Mol. Cell. Cardiol. 68 (2014) 98–105.
[41] J. Marin-Garcia, M.J. Goldenthal, G.W. Moe, Abnormal cardiac and skeletal muscle mitochondrial function in pacing-induced cardiac failure, Cardiovasc. Res. 52 (2001) 103–110.
[42] M. Schoepe, A. Schrepper, M. Schwarzer, M. Osterholt, T. Doenst, Exercise can induce temporary mitochondrial and contractile dysfunction linked to impaired respiratory chain complex activity, Metabolism 61 (2012) 117–126.
[43] H. Lemieux, S. Semsroth, H. Antretter, D. Hofer, E. Gnaiger, Mitochondrial respiratory control and early defects of oxidative phosphorylation in the failing human heart, Int. J. Biochem. Cell Biol. 43 (2011) 1729–1738.
[44] A. Hofer, T. Wenz, Post-translational modification of mitochondria as a novel mode of regulation, Exp. Gerontol. 56 (2014) 202–220.
[45] K. Shinmura, Post-translational modification of mitochondrial proteins by caloric restriction: possible involvement in caloric restriction-induced cardioprotection, Trends Cardiovasc. Med. 23 (2013) 18–25.
[46] N.V. Dudkina, R. Kouril, K. Peters, H.P. Braun, E.J. Boekema, Structure and function of mitochondrial supercomplexes, Biochim. Biophys. Acta 2010 (1797) 664–670.
[47] V. Beisvag, O.J. Kemi, I. Arbo, J.P. Loennechen, U. Wisloff, M. Langaas, et al., Pathological and physiological hypertrophies are regulated by distinct gene programs, Eur. J. Cardiovasc. Prev. Rehabil. 16 (2009) 690–697.
[48] I. Drozdov, A. Didangelos, X. Yin, A. Zampetaki, M. Abonnenc, C. Murdoch, et al., Gene network and proteomic analyses of cardiac responses to pathological and physiological stress, Circ. Cardiovasc. Genet. 6 (2013) 588–597.
[49] C. Riehle, A.R. Wende, Y. Zhu, K.J. Oliveira, R.O. Pereira, B.P. Jaishy, et al., Insulin receptor substrates are essential for the bioenergetic and hypertrophic response of the heart to exercise training, Mol. Cell. Biol. 34 (2014) 3450–3460.
[50] Y. Zhang, M. Yuan, K.M. Bradley, F. Dong, P. Anversa, J. Ren, Insulin-like growth factor 1 alleviates high-fat diet-induced myocardial contractile dysfunction: role of insulin signaling and mitochondrial function, Hypertension 59 (2012) 680–693.
[51] S. Javadov, V. Rajapurohitam, A. Kilic, J.C. Hunter, A. Zeidan, N. Said Faruq, et al., Expression of mitochondrial fusion–fission proteins during post-infarction remodeling: the effect of NHE-1 inhibition, Basic Res. Cardiol. 106 (2011) 99–109.
[52] J.M. Hollander, D. Thapa, D.L. Shepherd, Physiological and structural differences in spatially distinct subpopulations of cardiac mitochondria: influence of cardiac pathologies, Am. J. Physiol. Heart Circ. Physiol. 307 (2014) H1–14.